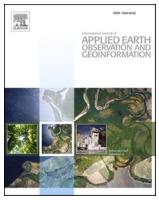
International Journal of Applied Earth Observation and Geoinformation 132 (2024) 104076



Contents lists available at ScienceDirect

International Journal of Applied Earth Observation and Geoinformation

journal homepage: www.elsevier.com/locate/jag



A hybrid model coupling PROSAIL and continuous wavelet transform based on multi-angle hyperspectral data improves maize chlorophyll retrieval

Anting Guo [a], Wenjiang Huang [a,c,*], Binxiang Qian [a,c], Huichun Ye [b], Quanjun Jiao [a], Xiangzhe Cheng [a,c], Chao Ruan [d]

[a] Key Laboratory of Remote Sensing and Digital Earth, Aerospace Information Research Institute, Chinese Academy of Sciences, Beijing 100094, China
[b] Key Laboratory of Digital Earth Science, Aerospace Information Research Institute, Chinese Academy of Sciences, Beijing 100094, China
[c] University of Chinese Academy of Sciences, Beijing 100049, China
[d] School of Internet, Anhui University, Hefei 230601, China

ARTICLE INFO

Keywords:
Maize
Chlorophyll retrieval
Multi-angle hyperspectral
PROSAIL
Continuous wavelet transform
Hybrid model

ABSTRACT

Chlorophyll is both a cornerstone of plant photosynthesis and an important indicator for assessing crop growth and health. Although many previous studies have explored the use of remote sensing to retrieve chlorophyll content, there is room for improvement in the proposed retrieval models, especially the hybrid model, and its performance in combination with multi-angle remote sensing remains unknown. To this end, we developed a hybrid chlorophyll retrieval model by coupling PROSAIL, Gaussian process regression, and continuous wavelet transform (CWT) based on multi-angle (−60° to 60°) hyperspectral observations of maize. The CWT converts PROSAIL-modeled and measured spectral reflectance into wavelet features (WF) that finely capture signals due to chlorophyll changes, making WF-based hybrid models (HMWF) promising for enhanced chlorophyll retrieval. Our results show that for leaf chlorophyll content (LCC) and canopy chlorophyll content (CCC) retrieval, combining low and medium scale WFs (scales3-5) with hybrid models is more advantageous than using other scale WFs. The accuracy of the HMWF based on the best-scale WF was significantly higher than that of the hybrid model based on original spectrum or vegetation indices. Additionally, our evaluation of the effect of viewing zenith angles (VZAs) on HMWF showed that the accuracies of HMWF acquired at non-nadir angles were generally higher than those acquired at nadir angle. Among all models, the HMWF based on the scale3 WF had the highest accuracy at −10°, with $R^2 = 0.85$ and RMSE=3.55 for LCC retrievals, and $R^2 = 0.78$ and RMSE=0.22 for CCC retrievals. Furthermore, the HMWF showed the least sensitivity to changes in VZAs, especially in the range of −10° to −40°. Overall, these findings highlight the effectiveness of HMWF with multi-angle hyperspectral data in improving chlorophyll retrieval accuracy. This study serves as a reference for crop parameter retrieval, crucial for advancing agricultural monitoring and management.

1. Introduction

Chlorophyll, as a core player in plant photosynthesis, is capable of absorbing light energy and converting it into biological energy, supporting plant growth, metabolism, and survival. It acts as a crucial marker for assessing plant growth and health (Sun et al., 2021). Traditionally, chlorophyll content is typically measured with high precision through on-site sample collection and chemical analysis based on plot samples. However, this method is associated with drawbacks such as high destructiveness, time-consuming procedures, and challenges in scaling up to large-scale accurate mapping (Zhen et al., 2021). Remote sensing technology, as a non-destructive monitoring technique, has emerged as the most feasible alternative to traditional chlorophyll measurement methods.

Remote sensing-based methods for chlorophyll retrieval in crops generally fall into three categories: (i) empirical statistical models that establish empirical relationships between chlorophyll and spectrum (Sinha et al., 2020). (ii) Physical models with a solid theoretical foundation and physical significance, including models such as Radiative Transfer Models (RTM) and Optical Models (Sinha et al., 2020; Li et al.,

* Corresponding author at: Key Laboratory of Remote Sensing and Digital Earth, Aerospace Information Research Institute, Chinese Academy of Sciences, Beijing 100094, China.
E-mail address: huangwj@aircas.ac.cn (W. Huang).

https://doi.org/10.1016/j.jag.2024.104076
Received 9 June 2024; Received in revised form 15 July 2024; Accepted 2 August 2024
Available online 8 August 2024
1569-8432/© 2024 The Author(s). Published by Elsevier B.V. This is an open access article under the CC BY-NC-ND license (http://creativecommons.org/licenses/by-nc-nd/4.0/).

2024). (iii) the hybrid model that combines RTM with machine learning algorithms. This model is both simple and physically grounded, making it widely used for inverting crop chlorophyll content (Verrelst et al., 2016). For example, Tagliabue et al. (2022) estimated chlorophyll, nitrogen and water content in crops by employing a hybrid model. Several pivotal components are essential for constructing hybrid retrieval methods for crop parameters: (i) RTM-based data simulation: PROSAIL, a combination of PROSPECT and SAIL, is widely used for generating simulation data due to its superior physicality and computational efficiency (Chakhvashvili et al., 2022). (ii) Machine learning algorithms for training simulated data: Commonly used machine learning algorithms include random forests, neural networks, and Gaussian process regression (GPR) (Sun et al., 2021). Notably, GPR offers advantages by requiring fewer training samples and providing meaningful uncertainty estimates (Estévez et al., 2022). (iii) Input features for machine learning algorithms: Input features often include the original spectrum (OS) (Tagliabue et al., 2022) directly generated by PROSAIL or vegetation indices (VIs) (Liang et al., 2015). Wavelet features (WFs) derived from original spectrum using the Continuous Wavelet Transform (CWT) have been widely used in crop parameter retrieval in recent years due to their ability to provide detailed information about the shape and location of spectral absorption features in vegetation (Wang et al., 2020). However, in most studies, WFs are typically obtained from measured spectral data for crop parameter inversion model construction (Li et al., 2018a). While this approach has shown better performance, it may suffer from poor model generalization. Combining CWT with RTM has great potential to solve this problem, especially when integrated with hybrid retrieval methods. This study aims to validate this idea. (IV) Optimization of models: Active Learning (AL) and Principal Component Analysis (PCA) are commonly used in hybrid models to optimize training datasets and mitigate issues related to spectral covariance, respectively (Candiani et al., 2022).

Currently, the spectral data essential for crop parameter retrieval is predominantly obtained from a single vertical direction. However, this approach is susceptible to the influence of soil background and vegetation canopy structure, consequently resulting in diminished retrieval accuracy (Wang et al., 2013). Compared with observation at nadir direction, multi-angle observation, which entails data collection from diverse viewing perspectives, proffers multidimensional crop information. This facet plays a pivotal role in encapsulating authentic surface reflection characteristics and spatial structures, thereby aiding in mitigating underdetermination and uncertainty in retrieval and, ultimately, elevating the precision of crop parameter retrieval (Kong et al., 2022). Multiple studies have used multi-angle observations in crop parameter retrieval studies. For instance, Wang et al. (2022) constructed new spectral indices for estimating cotton leaf nitrogen concentration based on multi-angle hyperspectral data acquired from ground-based equipment. He et al.(2016) and Guo et al.(2018) utilized various VIs to separately estimate Leaf Nitrogen Content and the stability of nitrogen absorption. Zhou et al. (2023) assessed the performance of vegetation indices obtained from different viewing zenith angles (VZAs) in estimating cotton nitrogen content. With the progressive evolution of UAV technology, the trend toward crop parameter retrieval based on multi-angle observations from UAV is gaining momentum (Lu et al., 2019). Moreover, certain satellite sensors, such as CHRIS-PROBA and MISR, are equipped with multi-angle observation capabilities. Researchers have leveraged the multi-angle data from these spaceborne sensors to conduct retrieval on parameters like chlorophyll content, LAI (Dorigo, 2011) and biomass (Wang et al., 2016). It is noteworthy that in the aforementioned studies, the predominant approach involves integrating multi-angle spectral data with empirical statistical methods for crop parameter retrieval. However, there has been limited attention given to the integration with RTM, particularly when combined with hybrid models.

Therefore, the main focus of this study was to develop a new hybrid model using ground-based multi-angle hyperspectral data to improve maize chlorophyll retrieval accuracy. The main goals were: (i) to verify the dominance of wavelet features in reflecting chlorophyll changes; (ii) to build the hybrid model that coupled by PROSAIL, machine learning and CWT to retrieve leaf chlorophyll content (LCC) and Canopy chlorophyll content (CCC) of maize; and (iii) to explore the effect of VZAs on the retrieval of maize chlorophyll. The results of this study will help to improve the level of monitoring of maize chlorophyll status using remote sensing methods, which is important for accurate monitoring of maize growth.

2. Materials and methods

2.1. Study area

We established two study areas to conduct multi-angle hyperspectral observation experiments on maize. Study Area 1 is the Shangzhuang Experimental Station of China Agricultural University in Haidian District, Beijing (E116°11′10″, N40°08′14.60″). Study Area 2 is the Science and Technology Innovation Demonstration Base of Beijing Academy of Agriculture and Forestry Sciences in Tongzhou District, Beijing (N116°40′42″, E39°41′43″) (Fig. 1). Haidian and Tongzhou Districts have temperate humid monsoon and continental monsoon climates, respectively, making them suitable for maize cultivation and growth. The dominant soil type in both study areas is brown soil, which is suitable for cultivating crops like wheat and maize. The maize growing season in both experimental areas spans from early June to late October.

2.2. Data acquisition

2.2.1. Field data

We conducted three experiments on June 25, July 8 and July 17, 2016, at the study area 1, resulting in a total of 55 sample datasets. Following that, on July 3 and July 13, 2023, we conducted two additional experiments at the study area 2, generating a total of 26 sample datasets. Maize sample data from various varieties were obtained across multiple periods and locations, providing a solid basis for verifying the generalizability of the chlorophyll retrieval model. LCC were measured at each sample point (1 × 1 m). The measurement of LCC involved the utilization of the SPAD-502 instrument (Konica Minolta, Tokyo, Japan) (Delegido et al., 2011). At each sample point, we selected three maize plants and averaged the measured SPAD values for all their leaves to obtain the SPAD value for that sample point. We used Equation (1) (Guo et al., 2023) to convert dimensionless SPAD values to chlorophyll content (mg/cm^2). The calculation of CCC is based on Equation (2) (Guo et al., 2023). Additionally, the geographic coordinates of each sample point were meticulously recorded using Differential Global Positioning System (DGPS).

$$LCC = 9.1411e^{0.0318*\mathrm{SPAD}} \quad (1)$$

$$CCC = LCC*LAI/100 \quad (2)$$

2.2.2. Multi-angle hyperspectral data

Multi-angle hyperspectral data for maize were acquired using an ASD FieldSpec Pro FR spectrometer (Analytical Spectral Devices, Boulder, CO, USA) (Fig. 2C). The ASD spectrometer's spectral range spans from 350 to 2500 nm (Mahlein et al., 2013). To enhance the precision of our spectral data, we used ASD's self-driven interpolation method to subdivide the spectra into 1 nm bandwidths (Yu et al., 2013). Atmospheric absorption bands ranging from 1320 to 1480 nm, 1750 to 2000 nm, and 2300 to 2500 nm were omitted before further processing. Furthermore, to align with simulated spectra, the range of 350–399 nm was excluded. The multi-angle bracket (Fig. 2A) is specifically designed for acquiring multi-angle hyperspectral data, comprising a manually operated rotational drive mechanism and a length-adjustable inverted L-shaped pole (Wu et al., 2021). The process of acquiring multi-angle hyperspectral data for maize involves first attaching the fiber-optic

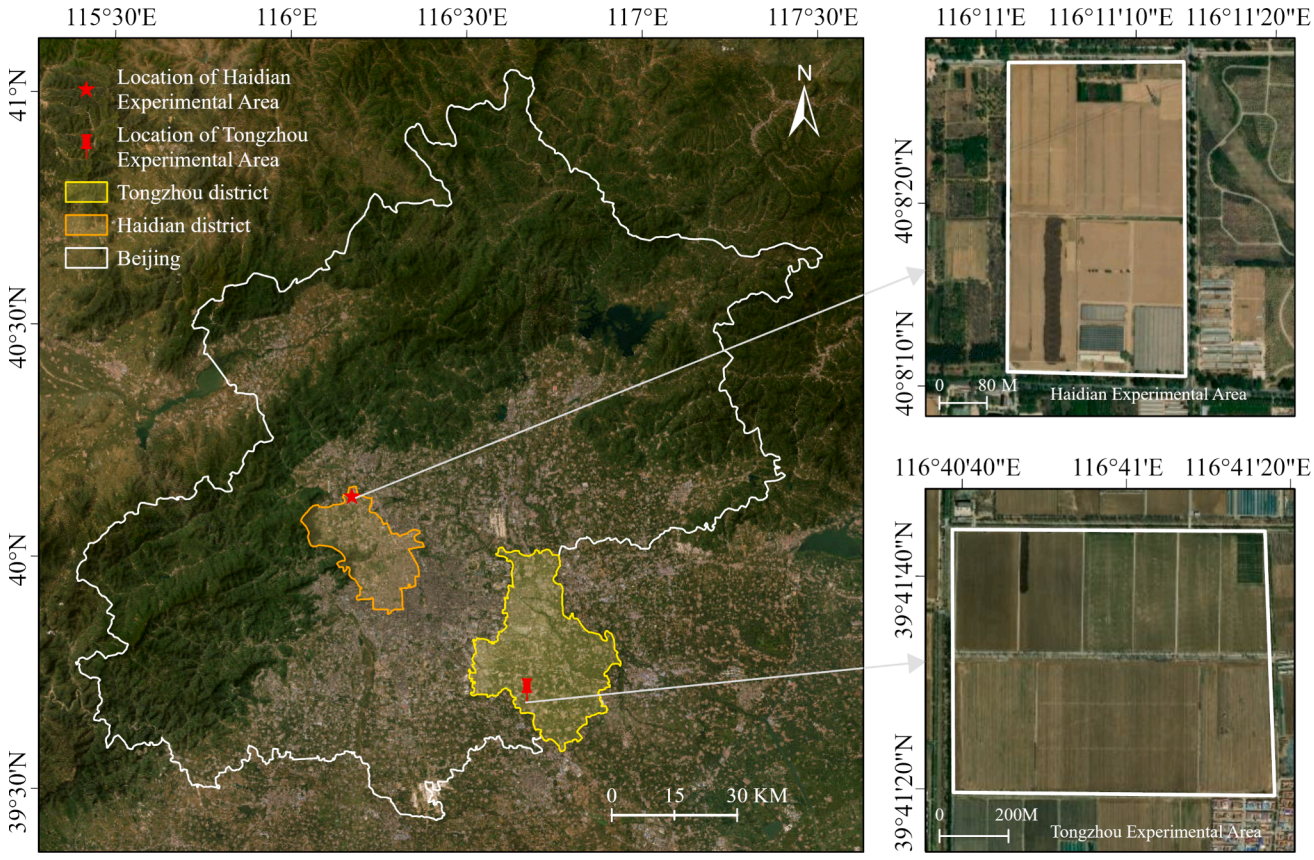


Fig. 1. Location of two study areas.

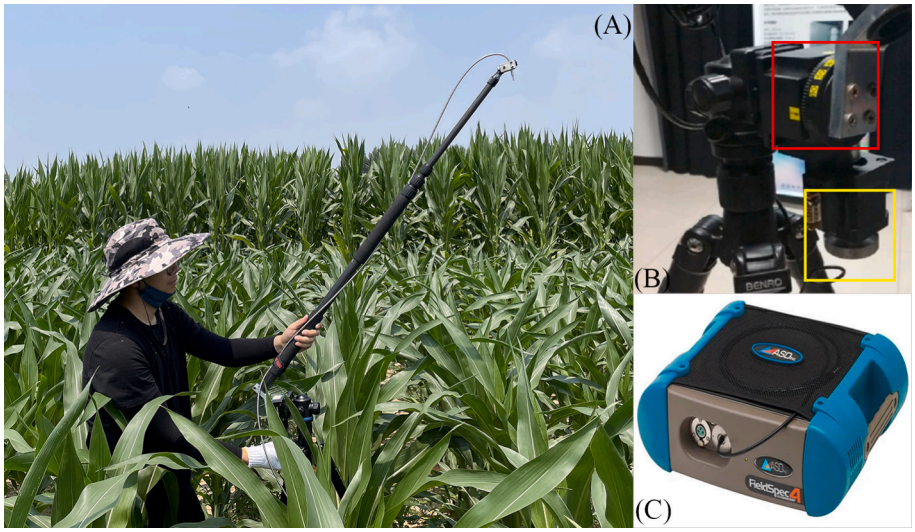


Fig. 2. Multi-angle hyperspectral measurements of maize. (A) illustrates the multi-angle hyperspectral measurement setup; (B) shows manual rotation drive mechanism; and (C) shows the ASD spectrometer.

probe connected to the ASD spectrometer to the upper end of the inverted L-shaped pole. The inverted L-shaped pole is then operated by manually rotating the drive mechanism's disc (yellow box in Fig. 2B) according to the number of degrees on the dial (red box in Fig. 2B), precisely controlling the swing of the fiber-optic probe to the desired viewing angle. Referring to the observation angle settings in previous studies (He et al., 2016; Guo et al., 2018; Zhang et al., 2021; He et al., 2022), we set up 13 VZAs along the solar principal plane to capture spectral data, ranging from −60° to + 60° at 10° intervals. Here, the negative sign (−) indicates the backscattering direction (on the same side as the sun), the positive sign (+) represents the forward scattering direction (on the opposite side of the sun), and measurements taken at the nadir direction are labeled as 0°. Spectral data at each angle were acquired within 30 s, and data for 13 angles were collected within 7 min. Additionally, spectra were gathered daily between 11:00 and 13:00 (local time UTC+8) to minimize the impact of light variations.

2.3. Construction and evaluation of the hybrid model for chlorophyll retrieval

The hybrid model is constructed by integrating the PROSAIL, GPR, AL, and CWT. Initially, we generated spectral data and corresponding chlorophyll content data using PROSAIL simulations. The spectral data were then transformed into wavelet features using CWT, and their quantitative relationship with chlorophyll content was established using GPR. Subsequently, techniques such as AL were used to optimize the sample data to construct parsimonious models. Finally, the hybrid model was applied to real multi-angle hyperspectral data to retrieve chlorophyll content. Notably, this study is the first to apply CWT in hybrid model construction combined with multi-angle hyperspectral data to retrieve chlorophyll content. Simultaneously, we also built OS-based (HMOS) and VI-based hybrid models (HMVI) separately as controls.

2.3.1. Acquisition of simulation data

Simulated data were obtained from the PROSAIL model fusing the leaf-level PROSPECT model and the canopy-level SAIL model (Verhoef et al., 2007). The PROSPECT-PRO within the PROSPECT model version simulates leaf directional-hemispherical reflectance and transmittance from 400 to 2500 nm at a 1 nm spectral resolution. Describing multiple scattering and radiative transfer processes within the canopy using the 4SAIL model. The input parameters of the PROSAIL model were set based on experimental measurements and values from the relevant literature, as shown in Table 1. Based on the input parameters, 2000 canopy reflectance in the range of 400 to 2500 nm and corresponding parameters were generated by forward simulation using the PROSAIL. The choice of 2000 samples are primarily to align with GPR that are well-suited for smaller sample sizes, consistent with previous studies (Tagliabue et al., 2022).

2.3.2. Continuous wavelet transform

The CWT aims to convert the spectral reflectance generated by the PROSAIL model into WFs, which can reflect chlorophyll changes more effectively. Essentially, CWT serves as a linear transformation method, utilizing wavelet basis functions to transform spectral reflectance into a series of wavelet coefficients at different scales (Zhang et al., 2020). Mathematically, the CWT is derived through scaling and shifting the mother wavelet function, with its calculation formula by following (Cheng et al., 2010):

$$\psi_{a,b}(\lambda) = \frac{1}{\sqrt{a}}\psi\left(\frac{\lambda - b}{a}\right) \tag{3}$$

where $\psi_{a,b}(\lambda)$ is the mother wavelet function. a and b are positive real numbers for the CWT, a represents the scaling factor defining the wavelet width, and b is the shifting factor determining the position. In this study, the commonly used the second derivative of Gaussian was employed as the mother wavelet function. The output results of the CWT are as follows (Cheng et al., 2011):

$$W_f(a,b) = \int_{-\infty}^{+\infty} f(\lambda)\psi_{a,b}(\lambda)d\lambda \tag{4}$$

where $W_f(a,b)$ are the wavelet coefficients, which includes the decomposition scale and the wavelength (Li et al., 2022) . Due to the high computational cost and data volume resulting from the CWT across a range of possible scaling factor (a = 1, 2, …, m), and the fact that the WFs obtained at high scales do not contain meaningful spectral information, decomposition of reflectance spectra is carried out only at binary scales such as 2^1, 2^2, 2^3, …, and 2^{10} (Rivard et al., 2008). The wavelet coefficients of these ten scales are denoted by WF1, WF2, …, WF10. Low scale WFs capture the narrower absorption features associated with chlorophyll, while high scale WFs describe the broad continuum in leaf reflectance spectra (Li et al., 2018b). The spectral width of the corresponding wavelet features increases with scale. Differences in chlorophyll uptake characteristics reflected by WFs at different scales allow hybrid models based on these features to produce varying results. The shifting factor determines the center wavelength of the shifted mother wave and is used to capture the peaks or valleys of the absorption features.$f(\lambda)$ represents the hyperspectral reflectance, λ is the spectral band number (λ = 1488). The spectrum ranges from 400 to 2500 nm, excluding the segments affected by water vapor absorption. Apart from transforming simulated spectral data generated by PROSAIL into WFs, we also converted field-measured spectral data into WFs for model validation. In this study, not only were the spectral data generated by PROSAIL transformed into WFs, but also the field-measured spectral data were converted into WFs for model validation.

2.3.3. Vegetation indices

We separately input the spectral reflectance produced by PROSAIL and the VIs derived from it into GPR to train the model. This process serves as a control for the WF-based hybrid model. Twelve commonly used VIs related to chlorophyll estimation were selected for this study (Table 2).

2.3.4. Gaussian process regression

GPR, by combining Bayesian theory with kernel methods, provides a powerful tool for addressing regression problems (Rasmussen, 2003). GPR offers three main advantages in crop parameters retrieval. First, uncertainty quantification: GPR not only provides predictions for crop parameters but also estimates the uncertainty associated with each prediction (Abdelbaki et al., 2021). Second, high flexibility: As a non-parametric model, GPR excels in handling complex and nonlinear relationships, demonstrating robust adaptability (Caicedo et al., 2014). Third, effectiveness with small sample sizes: GPR performs well even when trained on limited datasets (Guo et al., 2023).

2.3.5. Model optimization

Due to the potential redundancy in the spectral and WFs arising from their large quantity, PCA was employed to address the issue of collinearity in the hybrid model (Danner et al., 2021). We employ PCA to respectively condense sets of 1488 spectral features or WFs into 5 principal component (PC) bands or WFs. Additionally, given the possibility of redundant sample data among 2000 simulated samples, we utilize AL techniques for sample data optimization. AL can enhance the learning efficiency and performance of a model by selectively

Table 1
Parameter settings for the PROSAIL model in this study.

Model	Parameters	Description	Unit	Range
PROSPECT-PRO	N	Leaf structure	unitless	1–2
	LCC	Leaf chlorophyll content	ug/cm^2	10–70
	Car	Leaf carotenoid content	ug/cm^2	2–20
	C_{anth}	Leaf anthocyanin content	ug/cm^2	0–2
	EWT	Leaf water content	cm	0.001–0.02
	C_p	Leaf protein content	g/cm^2	0.001–0.0015
	C_{brown}	Brown pigment content	ug/cm^2	0–0.5
	CBC	Carbon-based constituents	g/cm^2	0.001–0.01
4SAIL	ALA	Average leaf angle	deg	20–70
	LAI	Leaf area index	m^2/m^2	1–6
	HOT	Hot spot parameter	m/m	0.01–0.5
	SZA	Solar zenith angle	deg	30
	OZA	Viewing zenith angle	deg	0–60
	RAA	Relative azimuth angle	deg	0/180
	BG	Soil brightness	unitless	0.8

Table 2
Formula and source of the VIs.

VIs	Formula	Reference
Triangular Vegetation Index (TVI)	$0.5(120(R_{750}-R_{550})-200(R_{670}-R_{550}))$	Broge and Leblanc, 2001
Modified Simple Ratio Index (MSR)	$(R_{750}/R_{705}-1)/sqrt(R_{750}/R_{705}+1)$	(Main et al., 2011)
Normalized Difference Vegetation Index (NDVI)	$(R_{800}-R_{670})/(R_{800}+R_{670})$	(Hunt et al., 2011)
Modified Triangular Vegetation Index (MTVI)	$1.2(1.2(R_{800}-R_{550})-2.5(R_{670}-R_{550}))$	(Haboudane et al., 2004)
Chlorophyll Index Red Edge (CIR)	$R_{750}/R_{710}-1$	(Gitelson et al., 2003)
Normalized Difference Red Edge Index1 (NDRE1)	$(R_{750}-R_{705})/(R_{750}+R_{705})$	Ehammer et al., 2010
Leaf Chlorophyll Index (LCI)	$(R_{850}-R_{710})/(R_{850}+R_{680})$	Datt, 1999
Modified Chlorophyll Absorption in Reflectance Index (MCARI)	$((R_{700}-R_{670})-0.2(R_{700}-R_{550}))(R_{700}/R_{670})$	Daughtry et al., 2000
Triangular chlorophyll index (TCI)	$1.2((R_{700}-R_{550})-1.5(R_{670}-R_{550})*\sqrt{(R_{700}/R_{670})}$	(Hunt et al., 2011)
Structure Intensive Pigment Index (SIPI)	$(R_{800}-R_{445})/(R_{800}-R_{680})$	Zarco-Tejada et al. (2001)
MERIS Terrestrial chlorophyll index (MTCI)	$(R_{754}-R_{709})/(R_{709}-R_{681})$	Dash, 2004
Vogelmann Red Edge Index 1 (VREI1)	R_{740}/R_{720}	(Vogelmann et al., 1993)

identifying and annotating the most informative data points. AL will be applied to the 2000 samples generated by the PROSAIL model, selecting the dataset that most effectively enhances model accuracy (Tagliabue et al., 2022). The Euclidean distance-based diversity (EBD) method demonstrated advantages in parameter retrieval and was consequently selected to optimize the model in this study (Verrelst et al., 2016). The GPR, PCA, and AL are all implemented within the Automated Radiative Transfer Models Operator (ARTMO) machine learning regression algorithm (MLRA) toolbox, accessible at https://artmotoolbox.com (Verrelst et al., 2020). Finally, the model was validated using a two-year measurement sample. The assessment criteria employed were the R^2 and RMSE indicators (De Grave et al., 2020).

3. Results

3.1. Changes in spectral reflectance and WFs under different chlorophyll contents and VZAs

The study compared variations in spectral reflectance and WFs under different LCC and CCC. LCC significantly influences spectral reflectance in the visible spectrum, with less impact in the near-infrared range (Fig. S1A). Specifically, in the 530–680 nm range, spectral reflectance decreases as LCC increases (Fig. 3A). Changes in WFs, especially in scales 1–5, are more detailed than spectral changes in the 500–800 nm range (Fig. S1B–F). For instance, WFs at scale 3 (WF3) show multiple increases or decreases as LCC increases (Fig. 3C). Regarding CCC, diverse CCC induce significant spectral changes from the visible to near-infrared region, with more pronounced variation in the near-infrared region (Fig. S2A). Aside from WF7-10, WFs at other scales show finer variations compared to spectral reflectance (Fig. S2). For instance, in the

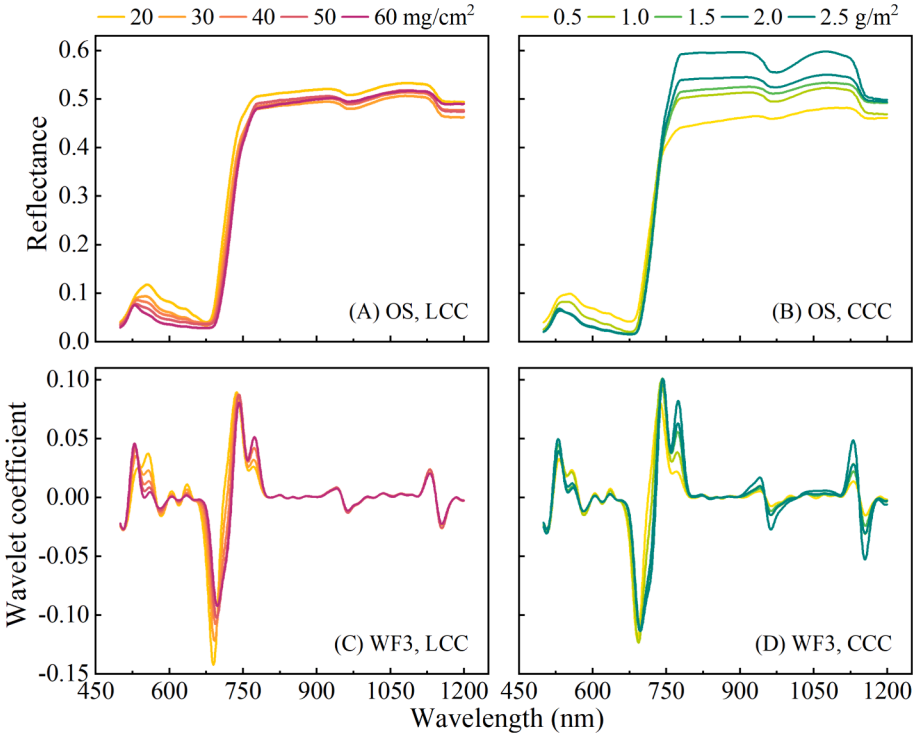


Fig. 3. The variations in spectral reflectance and WFs within the 500–1200 nm range under different chlorophyll contents. A-B depict the spectral changes induced by different LCC and CCC; C-D show the changes in WF3 resulting from different LCC and CCC.

500–1200 nm range, WF3 displays finer changes compared to spectral reflectance (Fig. 3D). These results suggest that CWT can effectively extract detailed information from spectral reflectance, particularly in medium and low-scale wavelet transformations, providing abundant features for chlorophyll retrieval.

We investigated the impact of VZAs on spectral reflectance and WFs, examining variations in six representative bands in the visible (450 nm, 560 nm, 670 nm) and near-infrared regions (800 nm, 970 nm, 1100 nm) under 13 VZAs (−60° to 60°). Spectral reflectance in the near-infrared region is significantly influenced by VZAs, while its impact on the visible region is comparatively minor. Additionally, VZAs in the backward scattering direction (−60° to −10°) have a more pronounced effect than those in the forward scattering direction (10° to 60°) (Fig. 4A and Fig. 4B). We also examined the variation of WFs derived from the six bands at different VZAs. Results indicate that WF3-7 exhibit minor variations within the −60° to 60° range, while WF1-2 and WF8-10 show slightly more pronounced changes (Fig. S3). Fig. 4C and Fig. 4D show the variation of WF3 at 13 VZAs. In summary, VZAs significantly impact the spectrum but have a relatively minor influence on WFs.

3.2. Chlorophyll retrieval of hybrid models based on WFs at different scales

Tables 3 and Table 4 show the LCC retrieval of the hybrid models based on WFs at scales 1–10 (HMWF1-10) for different VZAs (−60° to 60°). Overall, the LCC retrieval accuracy for the HMWF3-5 is significantly higher than that of HMWF at other scales. HMWF3 was the best performer among HMWF1-10, achieving the highest accuracy in 7 of the 13 VZAs. It also achieved the best performance of all models at −10° with $R^2 = 0.85$ and RMSE=3.55, and obtained R^2 above 0.8 from −40° to 0°. In addition to HMWF3, favorable results were also obtained for HMWF4, which achieved the highest accuracy in 4 out of 13 VZAs. HMWF5 achieves maximum accuracy at only one angle, −60°.

For the CCC retrieval, the research findings reveal that the HMWF3-4 significantly outperform the HMWF at other scale across the 13 VZAs (Table 5 and Table 6). Particularly, HMWF3 achieves the highest accuracy at 11 out of the 13 VZAs, with the remaining 2 VZAs showing the highest accuracy for the HMWF4. These results indicate that among the WF1-10, WF3-4 are more suitable for constructing CCC hybrid retrieval models.

3.3. Comparison of hybrid models based on different features

The performance of hybrid models incorporating different features (WF, OS, and VI) is evaluated for LCC and CCC retrievals across a range of VZAs (Table S1 and Table S2). Our findings indicate that HMWF consistently outperformed HMOS and HMVI across all 13 VZAs. For LCC retrieval, the R^2 values for HMWF3, HMWF4, and HMWF5 range from 0.66 to 0.85, 0.70 to 0.83, and 0.62 to 0.82, respectively, across the 13 VZAs. In contrast, the R^2 values for HMOS range from 0.50 to 0.78, and for HMVI range from 0.28 to 0.62. Fig. 5 presents scatter plots of the LCC retrieval results for the three models at selected VZAs. The R^2 of the HMWF3 model at −10° exceeds that of the HMOS and HMVI models by 0.07 and 0.24, respectively. Similarly, at 0°, the R^2 of the HMWF4 model surpasses that of the HMOS and HMVI models by 0.08 and 0.36, respectively. Similar results were observed for the CCC retrieval. Specifically, the accuracy of the HMWF3 and HMWF4 is significantly higher across all 13 VZAs compared to the HMOS and HMVI. For example, R^2 values for HMWF3 and HMWF4 range from 0.57 to 0.78 and 0.54 to 0.73, respectively. In comparison, the R^2 ranges for HMOS and HMVI are 0.14 to 0.48 and 0.10 to 0.44, respectively. In the scatter plot of CCC retrieval shown in Fig. 6, it is observed that the R^2 value for HMWF3 is 0.78 at −10°, which is 0.34 higher than the R^2 values for both HMOS and HMVI. Similarly, the R^2 value for HMWF4 is significantly higher than

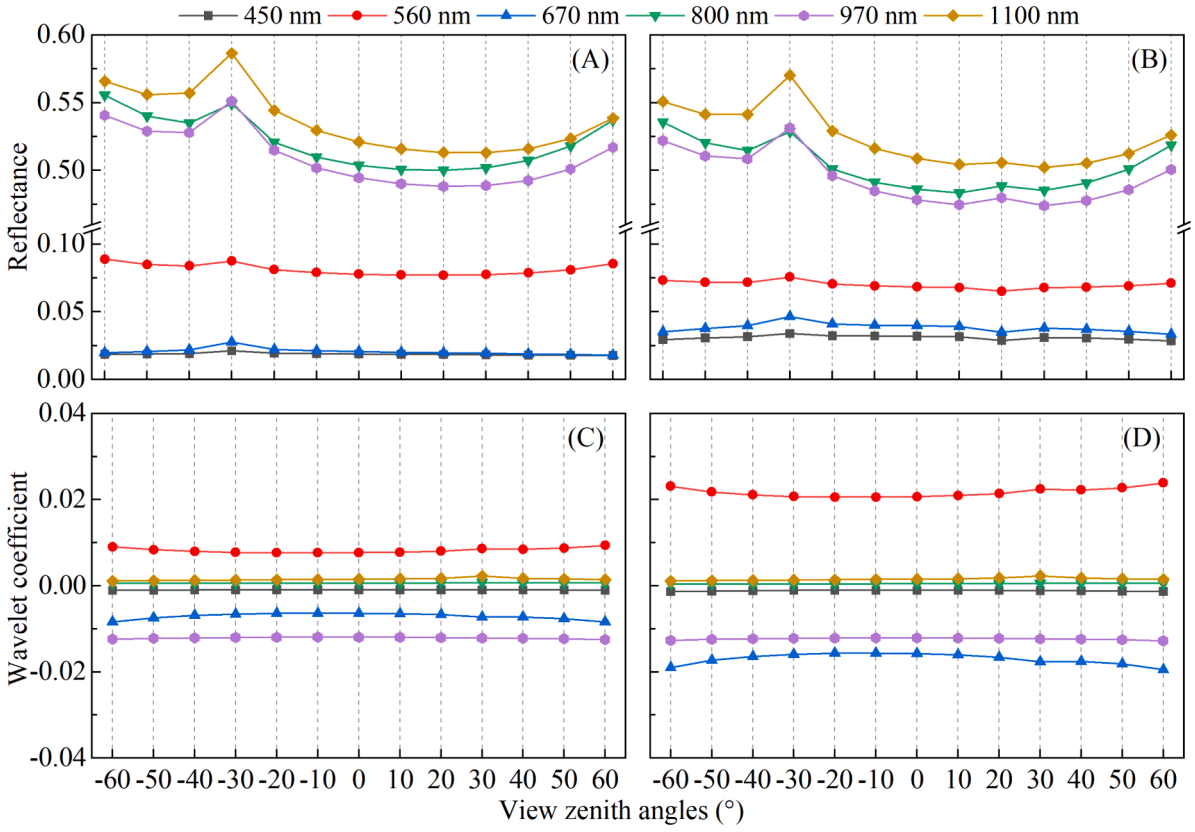


Fig. 4. Changes in spectral reflectance and WFs in different bands at various VZAs. A and B show the variation of the spectral reflectance under LCC and CCC, respectively. C and D show the variation of WF3 under LCC and CCC, respectively.

Table 3
The LCC retrieval results (R^2) for the HMWF1-10. Darker shades indicate higher accuracy (higher R^2).

Scale	-60°	-50°	-40°	-30°	-20°	-10°	0°	10°	20°	30°	40°	50°	60°
WF1	0.37	0.43	0.52	0.39	0.19	0.4	0.27	0.23	0.25	0.47	0.38	0.42	0.24
WF2	0.33	0.45	0.36	0.35	0.47	0.53	0.39	0.37	0.33	0.36	0.33	0.35	0.38
WF3	0.73	0.77	0.82	0.84	0.82	0.85	0.8	0.78	0.78	0.8	0.74	0.69	0.66
WF4	0.77	0.83	0.82	0.82	0.83	0.82	0.79	0.8	0.74	0.76	0.74	0.73	0.7
WF5	0.79	0.72	0.77	0.79	0.82	0.78	0.73	0.76	0.74	0.74	0.74	0.66	0.62
WF6	0.66	0.76	0.75	0.69	0.78	0.74	0.67	0.67	0.59	0.64	0.53	0.57	0.58
WF7	0.34	0.57	0.53	0.52	0.4	0.59	0.58	0.53	0.54	0.49	0.49	0.49	0.37
WF8	0.32	0.23	0.23	0.49	0.5	0.55	0.29	0.42	0.46	0.42	0.24	0.27	0.21
WF9	0.24	0.25	0.23	0.23	0.42	0.24	0.28	0.33	0.43	0.3	0.4	0.25	0.31
WF10	0.14	0.14	0.18	0.19	0.21	0.24	0.31	0.12	0.25	0.15	0.37	0.17	0.28

Table 4
The LCC retrieval results (RMSE) for the HMWF1-10. Darker shades indicate higher accuracy (lower RMSE).

Scale	-60°	-50°	-40°	-30°	-20°	-10°	0°	10°	20°	30°	40°	50°	60°
WF1	7.18	6.81	6.28	6.86	8.17	7.05	7.72	7.94	8.04	6.58	7.15	6.95	7.97
WF2	7.39	6.7	7.23	7.26	6.59	6.23	7.04	7.24	7.37	7.28	7.38	7.12	7.06
WF3	4.58	4.51	3.83	3.67	3.91	3.55	4.02	4.29	4.26	4.09	4.64	5.14	5.27
WF4	4.15	3.77	3.9	3.83	3.77	3.8	4.31	4.06	4.61	4.67	4.7	4.68	5.04
WF5	4.33	4.85	4.16	4.15	3.79	4.53	4.82	4.46	4.63	4.62	4.66	5.2	5.58
WF6	5.28	4.57	4.62	4.85	4.27	4.97	5.04	5.33	5.76	5.61	6.69	5.92	5.87
WF7	7.3	5.92	6.18	6.2	6.98	5.79	5.88	6.19	6.34	6.5	6.46	6.91	7.25
WF8	7.75	7.89	7.91	6.47	6.37	6.05	7.63	6.99	7.25	6.96	7.83	8.08	8.01
WF9	7.85	7.86	7.89	7.6	7.22	7.87	7.62	7.44	6.84	7.65	7.01	7.78	7.47
WF10	8.38	8.38	8.26	7.82	7.82	7.86	7.66	9.14	7.85	8.72	7.26	8.93	7.6

those of the other two models. For example, at −20°, the R^2 for HMWF4 is 0.20 and 0.28 higher than those for HMOS and HMVI, respectively. These findings suggest that integrating the WFs at the optimal scale with the hybrid model can significantly improve chlorophyll retrieval accuracy.

3.4. Impact of varying VZAs on the performance of HMWF

Fig. 7 and Fig. 8 illustrate the impact of different VZAs on the accuracy of HMWF for retrieving LCC and CCC, respectively. The results show that most HMWFs achieve higher accuracy in the off-nadir angles compared to the nadir angle (0°). For example, for LCC retrieval, HMWF3 has an R^2 of 0.82–0.85 at −40° to −10°, which is higher than the 0.8 at 0°. For CCC retrieval, HMWF3 is only lower than at 0° at −60°, 40°, 50°, and 60°, while surpassing the accuracy at 0° at all other VZAs. Additionally, the results indicate that the accuracy of HMWF is higher in the backward scattering direction than in the forward scattering direction. For example, for LCC retrieval, the R^2 values for HMWF3, HMWF4, and HMWF5 were 0.82, 0.83, and 0.82 at −20°, respectively, while at 20°, the R^2 values were only 0.78, 0.74, and 0.74. For CCC retrieval, the accuracy for HMWF3 at −30° is $R^2 = 0.75$, RMSE=0.23, while it is $R^2 = 0.65$, RMSE=0.27 at 30°. We find that HMWF performs better at small VZAs. Specifically, the highest model accuracies in both LCC and CCC retrievals are concentrated at −10° to −20°. For LCC retrieval, HMWF3 demonstrates the highest accuracy among all models at −10° with $R^2 = 0.85$ and RMSE=3.55. For CCC retrieval, HMWF3 also obtained the highest accuracy at −10° ($R^2 = 0.78$ and RMSE=0.22). Additionally, overall, CCC retrieval accuracy is lower than LCC retrieval accuracy. Specifically, the R^2 for the CCC retrieval using HMWF at the optimal scale ranges from 0.57 to 0.78 over the range of −60° to 60°, while the R^2 for LCC retrieval accuracy ranges from 0.73 to 0.85.

4. Discussion

4.1. The hybrid model based on WFs for chlorophyll retrieval

In this study, dimensionality reduction techniques, including PCA and AL, were integrated into the hybrid model to optimize its structure

Table 5
The CCC retrieval results (R^2) for the HMWF1-10. Darker shades indicate higher accuracy (higher R^2).

Scale	-60°	-50°	-40°	-30°	-20°	-10°	0°	10°	20°	30°	40°	50°	60°
WF1	0.1	0.12	0.22	0.2	0.21	0.15	0.29	0.12	0.16	0.24	0.29	0.2	0.27
WF2	0.36	0.28	0.32	0.3	0.28	0.43	0.31	0.41	0.3	0.3	0.22	0.25	0.22
WF3	0.62	0.73	0.69	0.75	0.71	0.78	0.64	0.66	0.71	0.65	0.6	0.64	0.57
WF4	0.6	0.62	0.72	0.72	0.68	0.73	0.63	0.61	0.65	0.69	0.52	0.57	0.54
WF5	0.53	0.49	0.63	0.61	0.65	0.58	0.48	0.56	0.56	0.45	0.47	0.5	0.48
WF6	0.48	0.51	0.53	0.55	0.58	0.56	0.47	0.5	0.48	0.43	0.48	0.5	0.45
WF7	0.42	0.49	0.43	0.47	0.46	0.43	0.38	0.5	0.44	0.41	0.41	0.42	0.39
WF8	0.22	0.4	0.39	0.34	0.41	0.32	0.32	0.47	0.33	0.41	0.37	0.32	0.25
WF9	0.39	0.38	0.39	0.31	0.34	0.39	0.26	0.4	0.36	0.27	0.24	0.25	0.26
WF10	0.31	0.22	0.36	0.39	0.3	0.25	0.2	0.15	0.14	0.18	0.15	0.13	0.27

Table 6
The CCC retrieval results (RMSE) for the HMWF1-10. Darker shades indicate higher accuracy (lower RMSE).

Scale	-60°	-50°	-40°	-30°	-20°	-10°	0°	10°	20°	30°	40°	50°	60°
WF1	0.46	0.45	0.41	0.43	0.43	0.44	0.38	0.48	0.47	0.43	0.41	0.44	0.42
WF2	0.36	0.39	0.38	0.41	0.39	0.34	0.38	0.35	0.38	0.47	0.4	0.4	0.43
WF3	0.28	0.24	0.25	0.23	0.24	0.22	0.27	0.27	0.25	0.27	0.29	0.27	0.3
WF4	0.29	0.29	0.24	0.24	0.26	0.24	0.28	0.29	0.34	0.25	0.32	0.3	0.31
WF5	0.31	0.33	0.34	0.29	0.33	0.29	0.33	0.3	0.3	0.4	0.33	0.33	0.33
WF6	0.33	0.32	0.31	0.3	0.3	0.32	0.33	0.32	0.33	0.34	0.33	0.33	0.34
WF7	0.35	0.32	0.35	0.34	0.33	0.34	0.37	0.32	0.34	0.35	0.35	0.42	0.35
WF8	0.4	0.35	0.35	0.39	0.37	0.38	0.4	0.33	0.37	0.36	0.37	0.38	0.4
WF9	0.36	0.37	0.39	0.38	0.39	0.36	0.41	0.39	0.36	0.39	0.43	0.4	0.39
WF10	0.38	0.42	0.37	0.35	0.39	0.4	0.42	0.42	0.42	0.46	0.54	0.52	0.39

and enhance accuracy. The number of PC features tends to impact model accuracy when compressing spectral bands using PCA techniques (Candiani et al., 2022). In this study, 1488 spectral bands or WFs were condensed into 5 PC features, resulting in strong model performance. Our other study on LAI retrieval confirmed the advantage of using 5 PC features over 20 (Guo et al., 2023). Furthermore, the AL technique was implemented to optimize the sample size. Among AL techniques, EBD stands out as a widely used method that significantly contributed to the superior results obtained by our model. However, recent research by Wocher et al. (2022) found that the variance-based pool of regressors (PAL) technique surpasses EBD in certain contexts, particularly in carbon content and biomass retrieval tasks. The different results may be due to the varying crops and parameters studied in the two studies. In the future, we will focus on further exploring the impact of different AL techniques on the hybrid model we constructed.

Our research results show that HMWF outperforms HMOS and HMVI. The reason for this improvement may lie in the use of Gaussian second-order derivatives as the mother wavelet of the CWT, which establishes similarities between each WF and the spectral reflectance at particular wavelength locations and scales (Cheng et al., 2011). This allows WFs to capture finer signal changes caused by chlorophyll (Fig. S1). In addition, we found that HMWF at mid-to-low scales (LCC: scales 3–5; CCC: scales 3–4) achieved the highest accuracy, while those based on low scales (1–2) and high scales (7–10) had lower accuracy. These results are consistent with the findings of Cheng et al.(2014). The reason for these results may be the increased noise in the WF1-2 and the coarser changes in the WF7-10 (Fig. S1 and Fig. S2), which are not able to capture the subtle changes in chlorophyll. Therefore, in future research on building chlorophyll retrieval models, it may be advisable to directly ignore low-scale (1–2) and high-scale (7–10) wavelet features. In addition, we observed that for HMWF3-6, the lower scale HMWF3-4 was more accurate than the higher scale HMWF5-6. Similar conclusions were found in the retrieval studies on parameters such as chlorophyll and water content by Feng et al. (2023). However, Li et al. (2017) found that the high scale was more favorable than the low scale in WF3-6. This discrepancy may be due to the fact that the two studies used WFs converted from spectra in different regions. They mainly used WFs obtained from spectra in the red-edge region for chlorophyll retrieval, while our

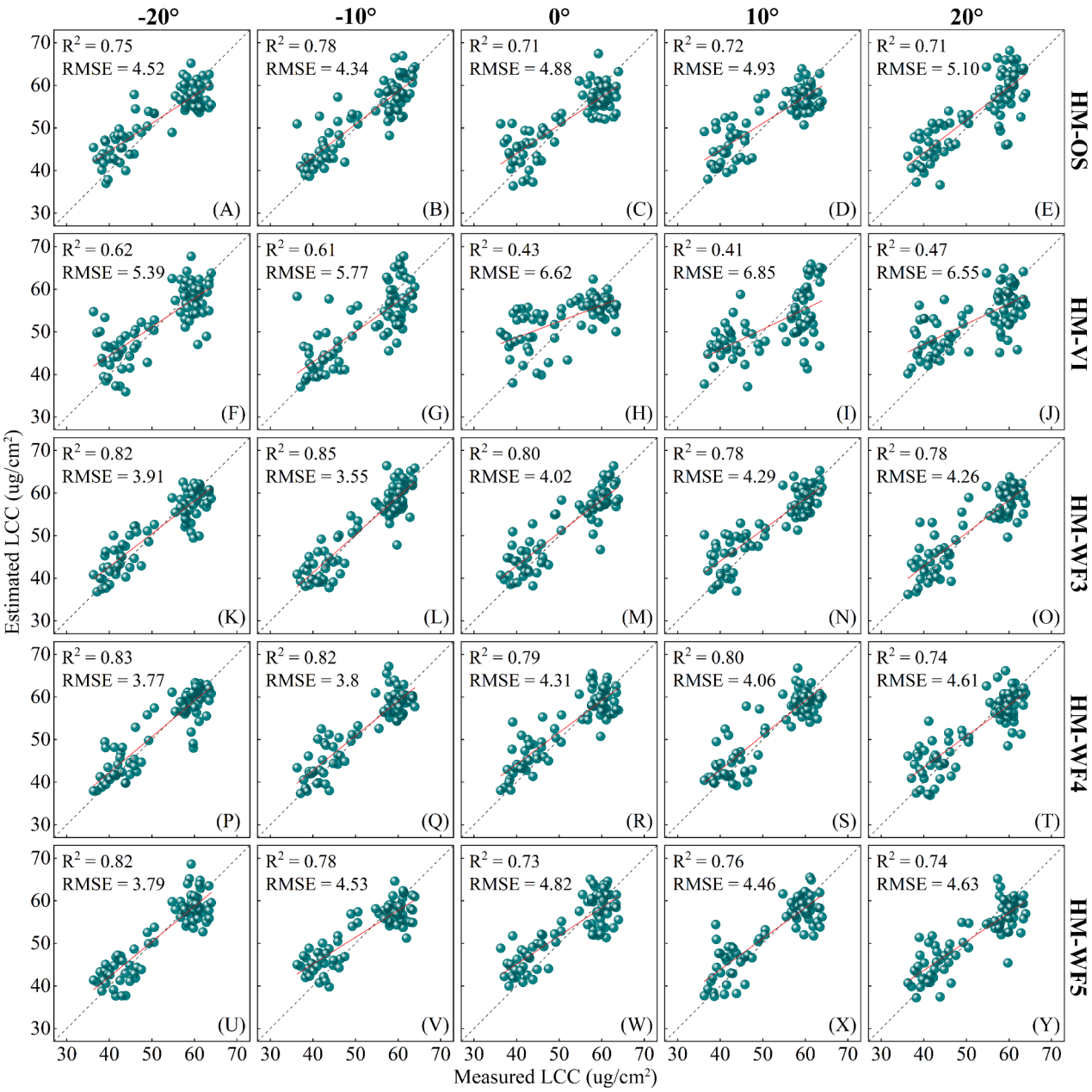


Fig. 5. The scatterplot compares the estimated LCC from hybrid models (A-E: HMOS, F-J: HMVI, K-O: HMWF3, P-T: HMWF4, U-Y: HMWF5) with measured LCC within the range of −20° to 20°.

study used WFs obtained from a wider range of spectra, from visible to near-infrared. Additionally, the different retrieval methods used in the two studies could also affect the results.

4.2. The impact of VZA on chlorophyll retrieval for hybrid models

Our results indicate that model accuracy is generally higher at off-nadir angles compared to nadir angles, especially at backscattering angles. This finding aligns with earlier research by Song et al. (2016). The primary reason is likely the significant impact of maize canopy gaps and soil background on spectral reflectance within the nadir field of view, which diminishes the contribution from the plants. Off-nadir observations reduce these impacts, facilitating more effective retrieval of vegetation information and improving model outcomes (Guo et al., 2018). Additionally, our study reveals that model accuracy at backscattering angles surpasses that at forward scattering angles. This phenomenon occurs because backscattering signals come from well-illuminated maize canopies, which are less affected by shadows. Thus, more signals from the leaves are detectable in backscattering measurements. Conversely, forward scattering signals come from shaded canopies, resulting in fewer detectable signals in forward scattering measurements. Similar results were observed in previous studies by He et al.(2022). We found that the VZAs for optimal performance of HMWF, HMOS, and HMVI are smaller angles, specifically −10° and −20°, which agrees with He et al. (2016) and Guo et al. (2018). This likely results from the strong light intensity and penetration depth into the crop canopy at these angles, facilitating comprehensive information acquisition from all crop layers and providing a holistic reflection of chlorophyll status (Li et al., 2020). Additionally, the HMWF model is generally less affected by VZAs. For example, in LCC retrieval, the R^2 values for HMWF 3–4 ranged from 0.82 to 0.85 within −10° to −40°. This may be due to the CWT technique converting spectra into WFs, resulting in less variability at different VZAs, particularly at scales 3–5 (Fig. S3).

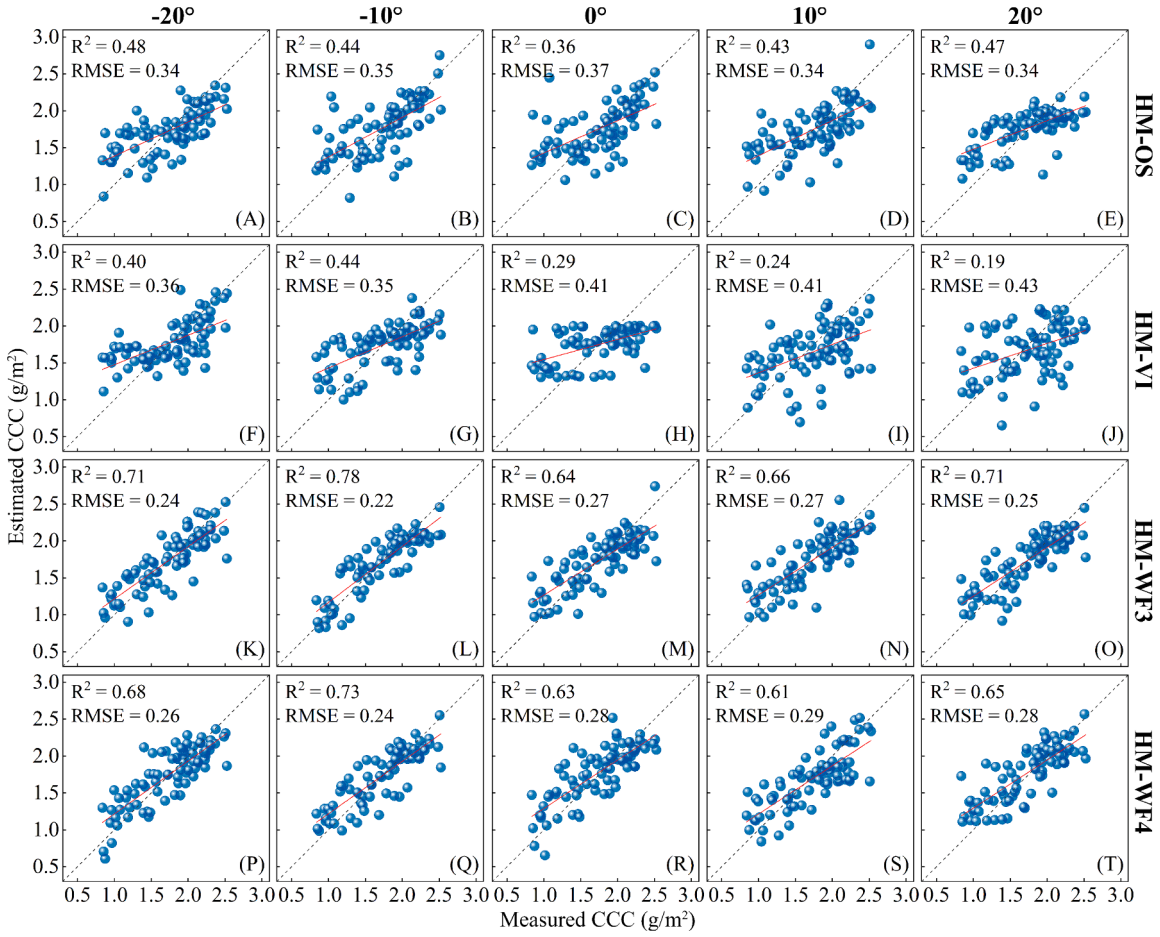


Fig. 6. The scatterplot compares the estimated CCC from hybrid models (A-E: HMOS, F-J: HMVI, K-O: HMWF3, P-T: HMWF4) with measured CCC within the range of −20° to 20°.

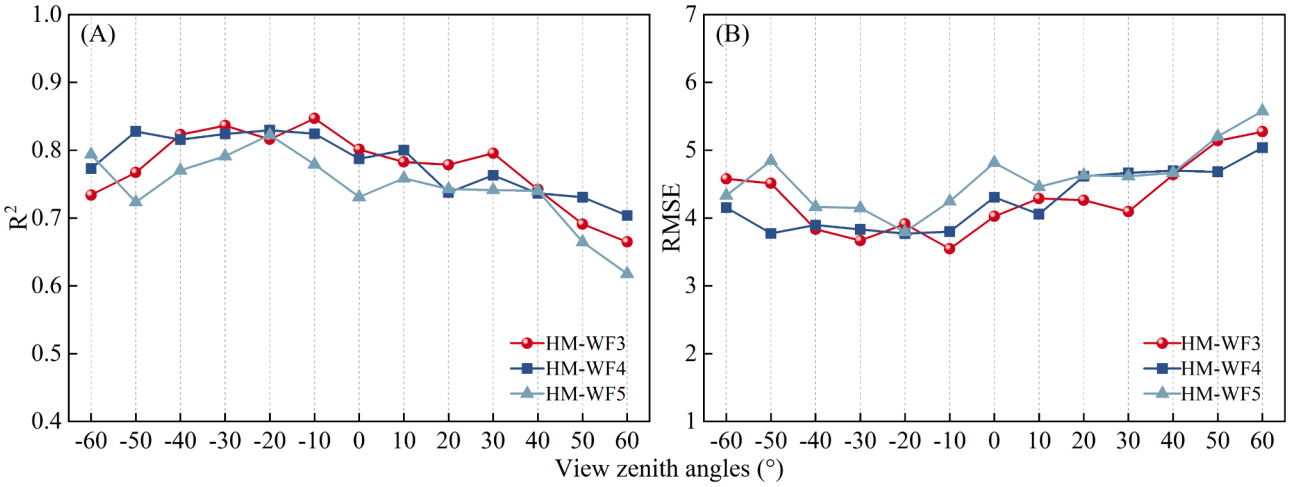


Fig. 7. The changes in LCC retrieval accuracy (A: R^2, B: RMSE) for HMWF3-5 in the range of −60° to 60°.

4.3. Challenges and outlook

In this study, we generated training data for the hybrid model using the PROSAIL model, which offers a certain level of generality. However, the PROSAIL model encounters challenges, such as the ill-posed inverse problem, a common issue in quantitative remote sensing (Verrelst et al., 2021). This problem could potentially impact our hybrid model, but we mitigated it by incorporating additional prior knowledge. To build a flexible and concise hybrid model, we used PROSAIL to generate 2000 simulation samples, a sample size previously chosen by Tagliabue et al. (2022) and Wocher et al. (2022). However, the amount of simulated data may affect the model's accuracy and speed. In future work, we aim to investigate the optimal balance between data quantity and model efficiency. Additionally, we plan to explore various advanced algorithms beyond GPR, such as deep learning, kernel ridge regression and adaptive boosting, to build stronger models. Angular interval selection is a key

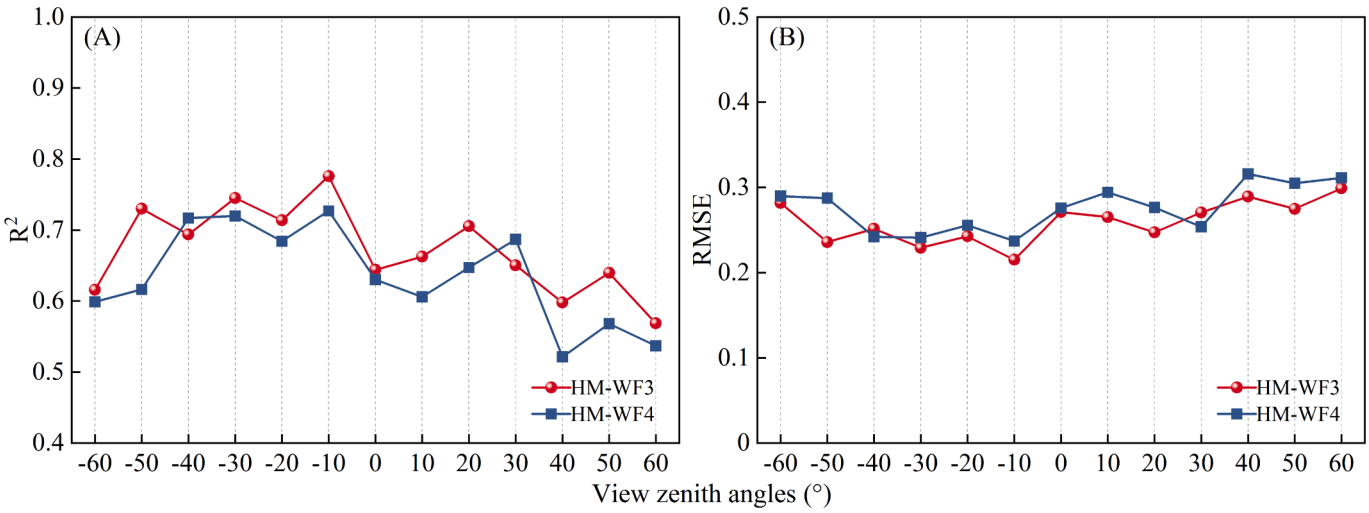


Fig. 8. The changes in CCC retrieval accuracy (A: R^2, B: RMSE) for HMWF3-4 in the range of −60° to 60°.

issue in multi-angle remote sensing observations. Referring to the previous studies (He et al., 2016; Guo et al., 2018; Zhang et al., 2021; He et al., 2022), we selected 13 angles with 10° intervals for chlorophyll retrieval. However, the effects of different angle intervals, such as 5°, 10°, 15°, and 20°, on the accuracy of chlorophyll retrieval have not been thoroughly investigated. We will explore this in the future. Although the hybrid model in this study was validated using datasets from two distinct study areas, enhancing the model's credibility and generalizability requires future validation with additional datasets. Additionally, the HMWF model we developed is primarily for maize, and its validity for other crops remains uncertain. In future studies, we will aim to extend the chlorophyll retrieval method proposed here to other crops, such as wheat and rice, to support crop growth monitoring.

In the future, we will extend the HMWF model to the UAV and satellite scales to enhance its usefulness. The application of the model at the UAV scale can promote precision agriculture, while the satellite scale can monitor crop growth over large areas and long time series, providing decision support for managers. However, we found that the inconsistency between the angles and generated spectral resolution of PROSAIL in the hybrid model and those in the satellite images limits the direct application of the constructed model to the satellite scale, especially for satellite multi-angle data. This problem can be solved by setting the angular parameters, spectral range, and resolution in the model to be consistent with those of the satellite sensors when generating simulated data using PROSAIL. Additionally, if the HMWF model is applied to satellite data with only a single vertical observation direction, there will be more room for its application at the satellite scale, especially for satellite hyperspectral data. A potential limitation of applying the HMWF model to satellite hyperspectral data is the need to convert satellite hyperspectral data to wavelet feature data using continuous wavelet transform for spatial mapping of maize chlorophyll, which may increase the model runtime. Furthermore, some common issues in crop parameter retrieval using satellite hyperspectral data may also appear in the model, such as atmospheric effects and mixed pixel problems.

5. Conclusion

In this study, we developed an innovative hybrid model by integrating CWT, PROSAIL, and GPR for the retrieval of maize chlorophyll. Our results show that in WF1-10, WFs at low and medium scales (LCC: scales 3–5; CCC: scales 3–4) have a significant advantage over WFs at other scales in constructing hybrid models. HMWF at optimal scales outperforms HMOS and HMVI, primarily due to its ability to capture finer signals caused by chlorophyll changes. Furthermore, an evaluation of the impact of VZAs on the hybrid models indicated that, for both LCC and CCC retrieval, HMWF at optimal scale generally exhibited higher performance at off-nadir angles compared to nadir angle. Additionally, the retrieval accuracy at backscattering angles surpassed that at forward scattering angles. The HMWF at optimal scale demonstrated less sensitivity to VZAs, particularly in the range of −10° to −40° (R^2 = 0.82–0.85). The HMWF showed optimal performance at −10° or −20°, suggesting that smaller VZAs are suitable for chlorophyll retrieval using the hybrid model. Notably, HMWF3 achieved the highest accuracy at −10° among all models, with retrieval accuracies of R^2 = 0.85 and RMSE=3.55 for LCC, and R^2 = 0.78 and RMSE=0.22 for CCC. These findings offer valuable insights for retrieving crop parameters utilizing multi-angle remote sensing across ground-based, UAV, and satellite platforms.

CRediT authorship contribution statement

Anting Guo: Writing – original draft, Visualization, Validation, Methodology, Investigation, Formal analysis, Conceptualization. **Wenjiang Huang:** Writing – review & editing, Supervision, Funding acquisition, Formal analysis. **Binxiang Qian:** Investigation, Formal analysis. **Huichun Ye:** Resources, Investigation. **Quanjun Jiao:** Software, Investigation. **Xiangzhe Cheng:** Software, Investigation. **Chao Ruan:** Software.

Declaration of competing interest

The authors declare that they have no known competing financial interests or personal relationships that could have appeared to influence the work reported in this paper.

Data availability

Data will be made available on request.

Acknowledgments

This article was supported by the National Key R&D Program of China (2023YFB3906202), the National Natural Science Foundation of China (42201365), Fengyun Application Pioneering Project (FY-APP-2022.0306), Hainan Province Science and Technology Special Fund (No. ZDYF2021GXJS038), and Technical Support Project for Malaria Control-Elimination in Sao Tome and Principe (3rd Round) (A2-6199-21-411-001).

Appendix A. Supplementary data

Supplementary data to this article can be found online at https://doi.org/10.1016/j.jag.2024.104076.

References

Abdelbaki, A., Schlerf, M., Retzlaff, R., Machwitz, M., Verrelst, J., Udelhoven, T., 2021. Comparison of crop trait retrieval strategies using UAV-based VNIR hyperspectral imaging. Remote Sens. [J] 13, 1748.

Broge, N.H., Leblanc, E., 2001. Comparing prediction power and stability of broadband and hyperspectral vegetation indices for estimation of green leaf area index and canopy chlorophyll density. Remote Sens. Environ. [j] 76, 156–172.

Caicedo, J.P.R., Verrelst, J., Muñoz-Marí, J., Moreno, J., Camps-Valls, G., 2014. Toward a semiautomatic machine learning retrieval of biophysical parameters. IEEE J. Sel. Top. Appl. Earth Observ. Remote Sens. [j] 7, 1249–1259.

Candiani, G., Tagliabue, G., Panigada, C., Verrelst, J., Picchi, V., Rivera Caicedo, J.P., Boschetti, M., 2022. Evaluation of hybrid models to estimate chlorophyll and nitrogen content of maize crops in the framework of the future CHIME mission. Remote Sens. [j] 14, 1792.

Chakhvashvili, E., Siegmann, B., Muller, O., Verrelst, J., Bendig, J., Kraska, T., Rascher, U., 2022. Retrieval of crop variables from proximal multispectral UAV image data using PROSAIL in maize canopy. Remote Sens. [j] 14, 1247.

Cheng, T., Rivard, B., Sánchez-Azofeifa, G., Feng, J., Calvo-Polanco, M., 2010. Continuous wavelet analysis for the detection of green attack damage due to mountain pine beetle infestation. Remote Sens. Environ. [j] 114, 899–910.

Cheng, T., Rivard, B., Sanchez-Azofeifa, A., 2011. Spectroscopic determination of leaf water content using continuous wavelet analysis. Remote Sens. Environ. [j] 115, 659–670.

Danner, M., Berger, K., Wocher, M., Mauser, W., Hank, T., 2021. Efficient RTM-based training of machine learning regression algorithms to quantify biophysical & biochemical traits of agricultural crops. ISPRS-J. Photogramm. Remote Sens. [j] 173, 278–296.

Dash J., Curran P. (2004). The MERIS terrestrial chlorophyll index.

Datt, B., 1999. Remote sensing of water content in Eucalyptus leaves. Australian Journal of Botany [j] 47, 909–923.

Daughtry, C.S., Walthall, C., Kim, M., De Colstoun, E.B., Mcmurtrey, I.J., 2000. Estimating corn leaf chlorophyll concentration from leaf and canopy reflectance. Remote Sens. Environ. [j] 74, 229–239.

De Grave, C., Verrelst, J., Morcillo-Pallarés, P., Pipia, L., Rivera-Caicedo, J.P., Amin, E., Belda, S., Moreno, J., 2020. Quantifying vegetation biophysical variables from the Sentinel-3/FLEX tandem mission: evaluation of the synergy of OLCI and FLORIS data sources. Remote Sens. Environ. [j] 251, 112101.

Delegido, J., Vergara, C., Verrelst, J., Gandía, S., Moreno, J., 2011. Remote estimation of crop Chlorophyll content by means of high-spectral-resolution reflectance techniques. Agron. J. [j] 103, 1834–1842.

Dorigo, W.A., 2011. Improving the robustness of cotton status characterisation by radiative transfer model inversion of multi-angular CHRIS/PROBA data. IEEE J. Sel. Top. Appl. Earth Observ. Remote Sens. [j] 5, 18–29.

Ehammer, A., Fritsch, S., Conrad, C., Lamers, J., Dech, S., 2010. Statistical derivation of fPAR and LAI for irrigated cotton and rice in arid Uzbekistan by combining multi-temporal RapidEye data and ground measurements[C]. Remote Sensing for Agriculture, Ecosystems, and Hydrology XII SPIE 66–75.

Estévez, J., Salinero-Delgado, M., Berger, K., Pipia, L., Rivera-Caicedo, J.P., Wocher, M., Reyes-Muñoz, P., Tagliabue, G., Boschetti, M., Verrelst, J., 2022. Gaussian processes retrieval of crop traits in Google Earth Engine based on Sentinel-2 top-of-atmosphere data. Remote Sens. Environ. [j] 273, 112958.

Feng, Z., Guan, H., Yang, T., He, L., Duan, J., Song, L., Wang, C., Feng, W., 2023. Estimating the canopy chlorophyll content of winter wheat under nitrogen deficiency and powdery mildew stress using machine learning. Comput. Electron. Agric. [j] 211, 107989.

Gitelson, A.A., Viña, A., Arkebauer, T.J., Rundquist, D.C., Keydan, G., Leavitt, B., 2003. Remote estimation of leaf area index and green leaf biomass in maize canopies. Geophys. Res. Lett. [j] 30.

Guo, A., Ye, H., Huang, W., Qian, B., Wang, J., Lan, Y., Wang, S., 2023. Inversion of maize leaf area index from UAV hyperspectral and multispectral imagery. Comput. Electron. Agric. [j] 212, 108020.

Guo, B.-B., Zhu, Y.-J., Feng, W., He, L., Wu, Y.-P., Zhou, Y., Ren, X.-X., Ma, Y., 2018. Remotely estimating aerial N uptake in winter wheat using red-edge area index from multi-angular hyperspectral data. Front. Plant Sci. [j] 9.

Haboudane, D., Miller, J.R., Pattey, E., Zarco-Tejada, P.J., Strachan, I.B., 2004. Hyperspectral vegetation indices and novel algorithms for predicting green LAI of crop canopies: Modeling and validation in the context of precision agriculture. Remote Sens. Environ. [j] 90, 337–352.

He, L., Song, X., Feng, W., Guo, B.-B., Zhang, Y.-S., Wang, Y.-H., Wang, C.-Y., Guo, T.-C., 2016. Improved remote sensing of leaf nitrogen concentration in winter wheat using multi-angular hyperspectral data. Remote Sens. Environ. [j] 174, 122–133.

He, L., Liu, M.-R., Guo, Y.-L., Wei, Y.-K., Zhang, H.-Y., Song, X., Feng, W., Guo, T.-C., 2022. Angular effect of algorithms for monitoring leaf nitrogen concentration of wheat using multi-angle remote sensing data. Comput. Electron. Agric. [j] 195, 106815.

Hunt Jr, E.R., Daughtry, C., Eitel, J.U., Long, D.S., 2011. Remote sensing leaf chlorophyll content using a visible band index. Agron. J. [j] 103, 1090–1099.

Kong, W., Huang, W., Ma, L., Li, C., Tang, L., Guo, J., Zhou, X., Casa, R., 2022. Biangular-combined vegetation indices to improve the estimation of canopy chlorophyll content in wheat using multi-angle experimental and simulated spectral data. Front. Plant Sci. [j] 13, 866301.

Li, D., Cheng, T., Zhou, K., Zheng, H., Yao, X., Tian, Y., Zhu, Y., Cao, W., 2017. WREP: A wavelet-based technique for extracting the red edge position from reflectance spectra for estimating leaf and canopy chlorophyll contents of cereal crops. ISPRS-J. Photogramm. Remote Sens. [j] 129, 103–117.

Li, D., Cheng, T., Jia, M., Zhou, K., Lu, N., Yao, X., Tian, Y., Zhu, Y., Cao, W., 2018a. PROCWT: Coupling PROSPECT with continuous wavelet transform to improve the retrieval of foliar chemistry from leaf bidirectional reflectance spectra. Remote Sens. Environ. [j] 206, 1–14.

Li, D., Chen, J.M., Zhang, X., Yan, Y., Zhu, J., Zheng, H., Zhou, K., Yao, X., Tian, Y., Zhu, Y., 2020. Improved estimation of leaf chlorophyll content of row crops from canopy reflectance spectra through minimizing canopy structural effects and optimizing off-noon observation time. Remote Sens. Environ. [j] 248, 111985.

Li, J., Ge, Y., Puntel, L.A., Heeren, D.M., Bai, G., Balboa, G.R., Gamon, J.A., Arkebauer, T. J., Shi, Y., 2024. Integrating UAV hyperspectral data and radiative transfer model simulation to quantitatively estimate maize leaf and canopy nitrogen content. Int. J. Appl. Earth Obs. Geoinf. [j] 129.

Li, L., Geng, S., Lin, D., Su, G., Zhang, Y., Chang, L., Ji, Y., Wang, Y., Wang, L., 2022. Accurate modeling of vertical leaf nitrogen distribution in summer maize using in situ leaf spectroscopy via CWT and PLS-based approaches. Eur. J. Agron. [j] 140, 126607.

Li, D., Wang, X., Zheng, H., Zhou, K., Yao, X., Tian, Y., Zhu, Y., Cao, W., Cheng, T., 2018b. Estimation of area-and mass-based leaf nitrogen contents of wheat and rice crops from water-removed spectra using continuous wavelet analysis. Plant Methods [j] 14, 1–20.

Liang, L., Di, L., Zhang, L., Deng, M., Qin, Z., Zhao, S., Lin, H., 2015. Estimation of crop LAI using hyperspectral vegetation indices and a hybrid inversion method. Remote Sens. Environ. [J] 165, 123–134.

Lu, N., Wang, W., Zhang, Q., Li, D., Yao, X., Tian, Y., Zhu, Y., Cao, W., Baret, F., Liu, S., 2019. Estimation of nitrogen nutrition status in winter wheat from unmanned aerial vehicle based multi-angular multispectral imagery. Front. Plant Sci. [J] 10, 1601.

Mahlein, A.-K., Rumpf, T., Welke, P., Dehne, H.-W., Plümer, L., Steiner, U., Oerke, E.-C., 2013. Development of spectral indices for detecting and identifying plant diseases. Remote Sens. Environ. [J] 128, 21–30.

Main, R., Cho, M.A., Mathieu, R., O'kennedy, M.M., Ramoelo, A., Koch S, S., 2011. An investigation into robust spectral indices for leaf chlorophyll estimation. ISPRS-J. Photogramm. Remote Sens. [J] 66, 751–761.

Rivard, B., Feng, J., Gallie, A., Sanchez-Azofeifa, A., 2008. Continuous wavelets for the improved use of spectral libraries and hyperspectral data. Remote Sens. Environ. [J] 112, 2850–2862.

Sinha, S.K., Padalia, H., Dasgupta, A., Verrelst, J., Rivera, J.P., 2020. Estimation of leaf area index using PROSAIL based LUT inversion, MLRA-GPR and empirical models: case study of tropical deciduous forest plantation, North India. Int. J. Appl. Earth Obs. Geoinf. [J] 86, 102027.

Song, X., Xu, D., He, L., Feng, W., Wang, Y., Wang, Z., Coburn, C.A., Guo, T., 2016. Using multi-angle hyperspectral data to monitor canopy leaf nitrogen content of wheat. Precis. Agric. [J] 17, 721–736.

Sun, Q., Jiao, Q., Qian, X., Liu, L., Liu, X., Dai, H., 2021. Improving the retrieval of crop canopy chlorophyll content using vegetation index combinations. Remote Sens. [J] 13, 470.

Tagliabue, G., Boschetti, M., Bramati, G., Candiani, G., Colombo, R., Nutini, F., Pompilio, L., Rivera-Caicedo, J.P., Rossi, M., Rossini, M., 2022. Hybrid retrieval of crop traits from multi-temporal PRISMA hyperspectral imagery. ISPRS-J. Photogramm. Remote Sens. [J] 187, 362–377.

Verhoef, W., Jia, L., Xiao, Q., Su, Z., 2007. Unified optical-thermal four-stream radiative transfer theory for homogeneous vegetation canopies. IEEE Trans Geosci. Remote Sensing [j] 45, 1808–1822.

Verrelst, J., Dethier, S., Rivera, J.P., Munoz-Mari, J., Camps-Valls, G., Moreno, J., 2016. Active learning methods for efficient hybrid biophysical variable retrieval. IEEE Geosci. Remote Sens. Lett. [J] 13, 1012–1016.

Verrelst, J., Berger, K., Rivera-Caicedo, J.P., 2020. Intelligent sampling for vegetation nitrogen mapping based on hybrid machine learning algorithms. IEEE Geosci. Remote Sens. Lett. [J] 18, 2038–2042.

Verrelst, J., Rivera-Caicedo, J.P., Reyes-Muñoz, P., Morata, M., Amin, E., Tagliabue, G., Panigada, C., Hank, T., Berger, K., 2021. Mapping landscape canopy nitrogen content from space using PRISMA data. ISPRS-J. Photogramm. Remote Sens. [J] 178, 382–395.

Vogelmann, J., Rock, B., Moss, D., 1993. Red edge spectral measurements from sugar maple leaves. TitleREMOTE SENSING [j] 14, 1563–1575.

Wang, Z., Chen, J., Fan, Y., Cheng, Y., Wu, X., Zhang, J., Wang, B., Wang, X., Yong, T., Liu, W., 2020. Evaluating photosynthetic pigment contents of maize using UVE-PLS based on continuous wavelet transform. Comput. Electron. Agric. [J] 169, 105160.

Wang, L., Dong, T., Zhang, G., Niu, Z., 2013. LAI retrieval using PROSAIL model and optimal angle combination of multi-angular data in wheat. IEEE J. Sel. Top. Appl. Earth Observ. Remote Sens. [J] 6, 1730–1736.

Wang, Q., Pang, Y., Li, Z., Sun, G., Chen, E., Ni-Meister, W., 2016. The potential of forest biomass inversion based on vegetation indices using multi-angle CHRIS/PROBA data. Remote Sens. [J] 8, 891.

Wang, J., Wang, H., Tian, T., Cui, J., Shi, X., Song, J., Li, T., Li, W., Zhong, M., Zhang, W., 2022. Construction of spectral index based on multi-angle spectral data for estimating cotton leaf nitrogen concentration. Comput. Electron. Agric. [J] 201, 107328.

Wocher, M., Berger, K., Verrelst, J., Hank, T., 2022. Retrieval of carbon content and biomass from hyperspectral imagery over cultivated areas. ISPRS-J. Photogramm. Remote Sens. [J] 193, 104–114.

Wu, B., Ye, H., Huang, W., Wang, H., Luo, P., Ren, Y., Kong, W., 2021. Monitoring the vertical distribution of maize canopy chlorophyll content based on multi-angular spectral data. Remote Sens. [J] 13.

Yu, K., Li, F., Gnyp, M.L., Miao, Y., Chen, X., 2013. Remotely detecting canopy nitrogen concentration and uptake of paddy rice in the Northeast China Plain. ISPRS-J. Photogramm. Remote Sens. [J] 78, 102–115.

Zarco-Tejada, P.J., Miller, J.R., Noland, T.L., Mohammed, G.H., Sampson, P.H., 2001. Scaling-up and model inversion methods with narrowband optical indices for chlorophyll content estimation in closed forest canopies with hyperspectral data. IEEE Trans. Geosci. Remote Sensing [j] 39, 1491–1507.

Zhang, H.-Y., Liu, M.-R., Feng, Z.-H., Song, L., Li, X., Liu, W.-D., Wang, C.-Y., Feng, W., 2021. Estimations of water use efficiency in winter wheat based on multi-angle remote sensing. Front. Plant Sci. [J] 12, 614417.

Zhang, J., Sun, H., Gao, D., Qiao, L., Liu, N., Li, M., Zhang, Y., 2020. Detection of canopy chlorophyll content of corn based on continuous wavelet transform analysis. Remote Sens. [J] 12, 2741.

Zhen, J., Jiang, X., Xu, Y., Miao, J., Zhao, D., Wang, J., Wang, J., Wu, G., 2021. Mapping leaf chlorophyll content of mangrove forests with Sentinel-2 images of four periods. Int. J. Appl. Earth Obs. Geoinf. [J] 102.

Zhou, X., Yang, M., Chen, X., Ma, L., Yin, C., Qin, S., Wang, L., Lv, X., Zhang, Z., 2023. Estimation of cotton nitrogen content based on multi-angle hyperspectral data and machine learning models. Remote Sens. [J] 15, 955.